Journal of Physics: Condensed Matter

PAPER

Tunable magnetic low-frequency noise in magnetic tunnel junctions: effect of shape anisotropy

To cite this article: Xu Li *et al* 2020 *J. Phys.: Condens. Matter* **32** 495805

IOP Publishing Journal of Physics: Condensed Matter
J. Phys.: Condens. Matter **32** (2020) 495805 (9pp) https://doi.org/10.1088/1361-648X/abb443

Tunable magnetic low-frequency noise in magnetic tunnel junctions: effect of shape anisotropy

Xu Li[1,5], Chao Zheng[2,5], Edmund R Nowak[3], Kevin Haughey[3], Robert D Shull[4], P J Chen[4] and Philip W T Pong[2,*]

[1] Fujian Provincial Key Laboratory of Semiconductors and Applications, Collaborative Innovation Center for Optoelectronic Semiconductors and Efficient Devices, Department of Physics, Xiamen University, Xiamen 361005, People's Republic of China
[2] Department of Electrical and Electronic Engineering, The University of Hong Kong, Hong Kong Special Administrative Region of China
[3] Department of Physics and Astronomy, University of Delaware, Newark, Delaware 19716, United States of America
[4] Functional Nanostructured Materials Group, National Institute of Standards and Technology, Gaithersburg, MD 20899-8552, United States of America
[5] These authors contributed equally to this work.

E-mail: ppong@eee.hku.hk

Received 18 April 2020, revised 12 August 2020
Accepted for publication 1 September 2020
Published 17 September 2020

Abstract

The intrinsic magnetic low-frequency noise (LFN) is of fundamental scientific interest to the study of magnetic tunnel junctions (MTJs). To gain insight into its mechanism, the fluctuation-dissipation theorem, which describes the linear relation between magnetic LFN and magnetic sensitivity product, has been utilized. However, deviation from the linear correlation has been reported in some studies. To understand and effectively control the magnetic LFN, a more elaborate analytical description and further experimental validation are required. In this work, the magnetic LFN contributed from the magnetization fluctuation in the pinned layer of MTJs with various shape anisotropies was investigated. The MTJs with different shape anisotropies, achieved by altering their aspect ratios, possessed distinct demagnetizing factors. Large magnetic noise was correlated with the increase of magnetic phase loss of ferromagnetic layers during magnetization reversal at which magnetization fluctuation was enhanced. Upon increasing the shape anisotropy, a notable reduction of the magnetic phase loss in the antiparallel (AP) state was observed while it exhibited a slight decrease in the parallel (P) state, revealing that the increase of the shape anisotropy caused a more pronounced suppression of the equilibrium magnetization fluctuation in the AP state. These phenomena were computationally validated by constructing a macrospin model to describe the thermally-induced magnetization fluctuation in the pinned layer. This work reveals the physical relation between MTJ shape anisotropy and magnetic LFN. The effect of the shape anisotropy on the magnetic LFN can be extended to other types of in-plane uniaxial anisotropies.

Keywords: magnetic tunnel junction, magnetic low-frequency noise, magnetic shape anisotropy

* Author to whom any correspondence should be addressed.

S Supplementary material for this article is available online

(Some figures may appear in colour only in the online journal)

Nomenclature

α_{mag}	Hooge parameter
AP	antiparallel
ε_{mag}	magnetic phase loss
FDT	fluctuation-dissipation theorem
H_{sa}	shape anisotropy
LFN	low-frequency noise
MSP	magnetic sensitivity product
MRTN	magnetic random telegraph noise
MTJs	magnetic tunnel junctions
P	parallel
RevP	reversed parallel
TMR	tunnel magnetoresistance

1. Introduction

Magnetic tunnel junctions (MTJs) have drawn attention in many applications such as magnetic random-access memories and magnetic field sensors owing to their sensitive response to external excitations [1–8]. One of the major limitations for the performance of MTJ-based devices is their relatively high intrinsic noise [7, 9–11]. Particularly at low frequency, the intrinsic magnetic low-frequency noise (LFN) has a large magnitude in the antiparallel (AP) state and during the magnetic reversal process of magnetic layers [10–14]. To understand and effectively control the magnetic LFN, both theoretical and experimental works have been carried out [11, 15–20]. The LNF of MTJs could be reduced by engaging magnetic flux concentrators [21, 22], voltage bias [23], and magnetic shielding [24], or by modifying the magnetic materials [20], underlayer structure [25] and MTJ shapes [26]. However, while these strategies were proved to be effective for noise reduction, the origin of magnetic noise remains not well understood. Further research is required to explore for the intrinsic properties of magnetic noise in MTJs.

In MTJs, the magnetization fluctuation in ferromagnetic layers can induce resistance changes, which is manifested as voltage noise when MTJs are current-biased [27]. Using the fluctuation-dissipation theorem (FDT), the magnetic LFN can be related to the magnetic sensitivity product (MSP) of the MTJ and the magnetic phase loss (dissipation) of the corresponding magnetic layer [18, 28, 29]. Usually, the magnetic LFN is linearly proportional to the MSP in thermal equilibrium, giving rise to the field-independent magnetic phase loss [26, 30]. However, the deviation from the linear behaviour between the MSP and magnetic LFN has been reported in the literature as well [11, 18, 27]. This discrepancy lies in two major causes: (1) the involvement of the magnetic random telegraph noise (MRTN) that introduces extra magnetic noise [10, 11, 31, 32], (2) the presence of magnetic inhomogeneities (e.g., magnetic ripples and disorders) that lead to discrete magnetization jumps [18, 27, 32]. Although experiments show the magnetic LFN is correlated with the magnetic phase loss, a more complete analytical description and further experimental validation are lacking. Besides, the magnetic noise power spectra of an MTJ is a superposition of noise from the uncorrelated fluctuation of both the free layer and the pinned layer [33]. The contribution of the pinned-layer fluctuation is even more pronounced in the AP state [11, 34]. While most of the previous research investigated the noise of MTJs by considering only the fluctuation of the free layer while assuming the pinned-layer magnetization is frozen, the character of the pinned-layer-related noise is rarely reported.

In this work, the magnetic LFN of MTJs were investigated under large negative magnetic field. The adoption of such field range suppressed the fluctuation of the free layer and guaranteed the dominant role of pinned-layer fluctuation as the noise source. The varied shape anisotropies were introduced to tailor the magnetic LFN of MTJs. The experimental observations were analyzed by constructing a macrospin model. The experimental results and the analytical model confirmed a strong correlation between the magnetic phase loss and LFN, while both factors could be effectively tuned by magnetic shape anisotropy. This work has unravelled the physical mechanism of magnetic LFN originated from the magnetization fluctuation of the pinned layer.

2. Experimental methods

The MTJ thin films were deposited on thermally oxidized silicon substrates by magnetron sputtering. The base pressure of the processing chamber was 2.66×10^{-7} Pa (2×10^{-9} Torr). The structure of the prepared MTJ stacks was as follows (units in angstroms): substrate/NiFeCuMo (200)/CoFe (10)/Al (10) + plasma oxidization/CoFe (10)/NiFeCuMo (25)/CoFe (5)/IrMn (100)/Ru (70). The Al oxide tunnel barrier was formed by depositing a metal Al layer and subsequently oxidizing it in a pure O_2 plasma. After the deposition of the MTJ thin films, the samples were annealed at 200 °C for 15 min with a 70 mT magnetic field applied parallel to the film plane. The MTJ thin films were then patterned to elliptical tunnel junctions, shown in figure 1, by utilizing photolithography and etching techniques. The long axis of the ellipse is patterned along the direction of the annealing field so that the exchange bias field of the pinned layer is parallel to the easy axis of

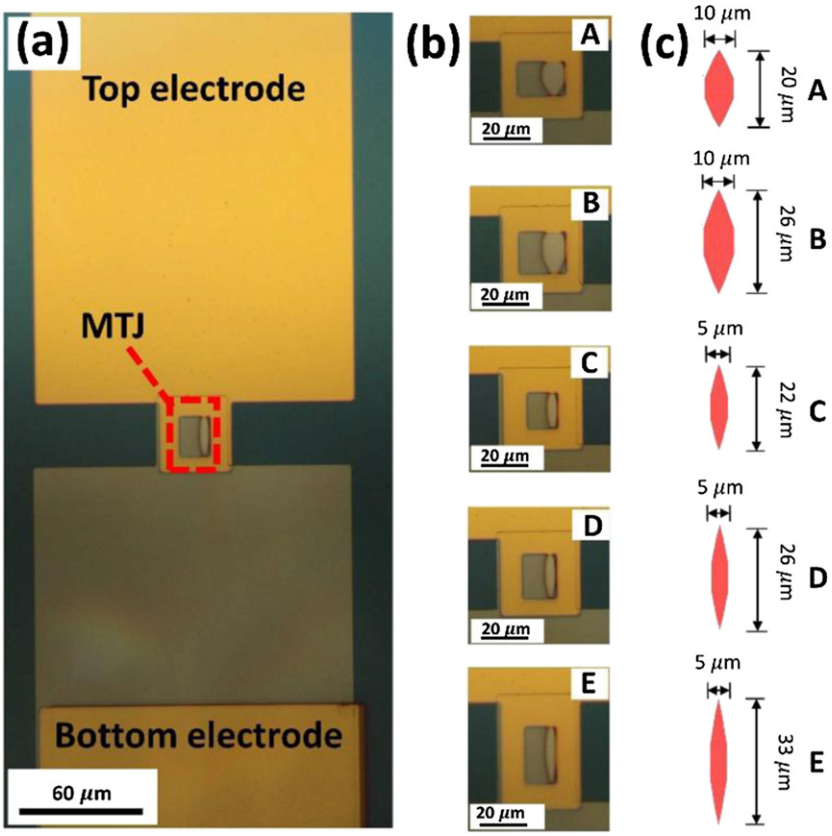

Figure 1. Optical images of the MTJ (a) and closeups of the MTJ devices (b). Panel (c) shows schematics of the MTJ geometries.

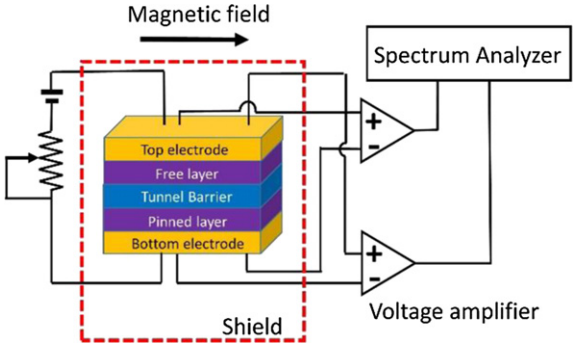

Figure 2. Schematic of the experimental setup for noise measurement.

the free layer. The MTJ junctions were patterned from the same MTJ wafer to eliminate the experimental difference and ensure the coherence of the noise measurement. Five groups of MTJs with different aspect ratios were fabricated, whose optical images and schematics are illustrated in figures 1(b) and (c), respectively. The tunnel magnetoresistance (TMR) curves of the MTJs were measured by using a four-probe method with the magnetic field applied along the long axis of the elliptical MTJs.

The noise measurements were carried out in a metal enclosure to suppress the external noise sources, as depicted in figure 2. A battery and variable resistor were utilized to provide a constant bias current. Two low-noise voltage amplifiers (FEMTO DLPVA-100-BLN-S[6]) were connected in parallel across the MTJ and their outputs were fed into a dual-channel spectrum analyzer (HP 35670A[6]). A cross-correlation method was used to reduce the uncorrelated amplifier and external noise sources. Low-frequency spectra were measured from 0.1 kHz to 10 kHz under the high-resistance and low-resistance states of the MTJ. To eliminate the transient effects (e.g., out-of-equilibrium effects associated with the magnetic aftereffect [17]), each noise measurement was started after the MTJ resistance had stabilized at least 10 min after the external magnetic field was changed (supplementary material (https://stacks.iop.org/JPCM/32/415805/mmedia)). The noise power spectrum density was averaged for 1000 times by the internal fast averaging function. The frequency spectrum of the magnetic LFN (S_V^{mag}) was obtained by subtracting the contributions of the thermal noise, shot noise, electronic 1/*f* noise, amplifier noise, and system background noise from the measured one [26, 35] (supplementary material). To compare the magnetic LFN in different MTJs, the LFN was parametrized by a Hooge-like expression [18, 34]:

$$\alpha_{\mathrm{mag}} = \frac{\Omega f^{\beta} S_V^{\mathrm{mag}}}{V^2}, \tag{1}$$

where α_{mag} is the Hooge parameter, Ω is the volume of the

[6] Disclaimer: the use of manufacturer names and trademarks are only for the purpose of completely describing the experimental conditions and does not imply an endorsement of the authors or their organizations.

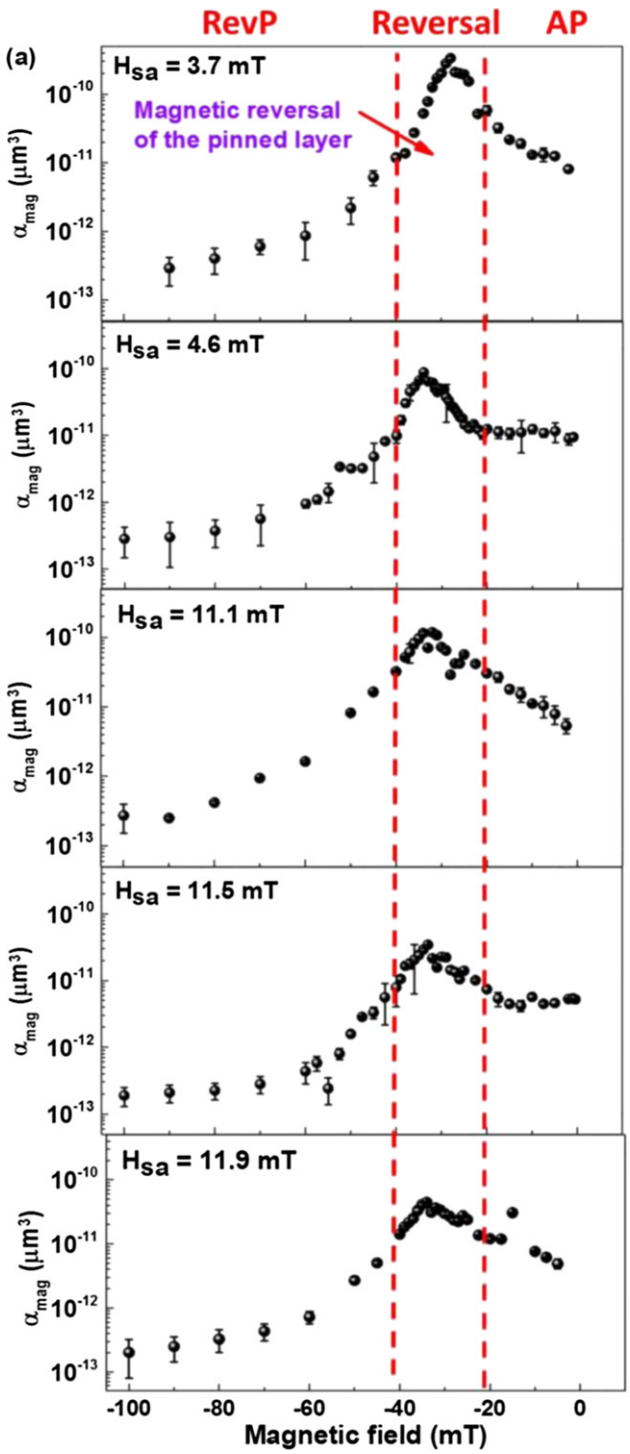

Figure 3. (a) Typical magnetoresistance curve of MTJ with the in-plane easy-axis magnetic field sweeping from −100 mT to +10 mT, (b) magnetic-field-dependence of the measured Hooge parameter (α_{mag}), (c) magnetic-field-dependence of MSP, (d) magnetic-field-dependence of the magnetic phase loss (ε_{mag}).

corresponding magnetic layer, f is the frequency, β is the exponent, and V is the applied voltage. All the measurements were performed at room temperature.

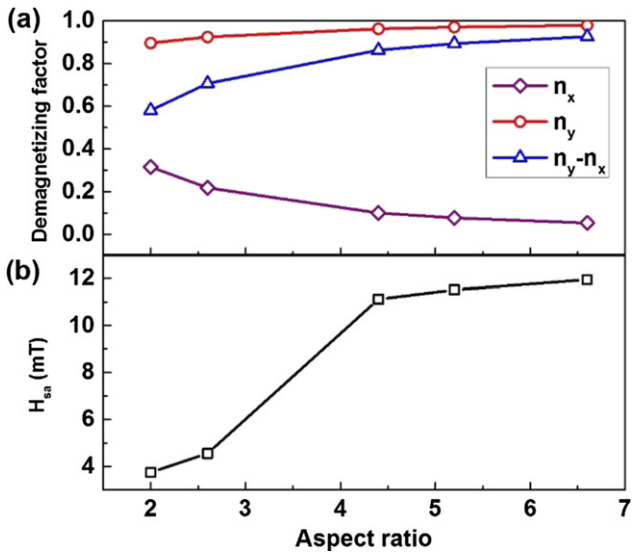

Figure 4. (a) Demagnetizing factors with respect to the aspect ratio (u) of the MTJs, (b) shape anisotropy (H_{sa}) of the pinned layer with respect to the aspect ratio (u) of the MTJs.

3. Experimental results

The magnetic-field-dependence of the MTJ resistance and noise were characterized, as shown in figure 3. A typical TMR curve is illustrated in figure 3(a), which was obtained by sweeping the applied magnetic field from −100 mT to +10 mT. The magnetic state was switched from the reversed parallel (RevP) to AP magnetization configuration and back to the normal parallel (P) state. Between −40 mT and −20 mT, the MTJ resistance gradually increases, indicating that the pinned layer was undergoing a magnetic reversal process. The magnetic LFN of the MTJ was extracted and the corresponding Hooge parameter (α_{mag}) was determined using equation (1). For all measured noise spectra, no Lorentzian features were identified and the exponent (β) was close to 1, revealing that no MRTN was involved in the measured noise [30]. The extracted noise was notably dependent on the magnetization configuration, which confirmed its magnetic origin [36–38]. The measured magnetic noise is attributed to the magnetization fluctuation of the pinned layer, because the magnetization of the free layer was presumably fixed for the applied magnetic field ranging from −100 mT to −2 mT, while the magnetization of the pinned layer switched within the field range of −20 mT to −40 mT. This assumption is supported by the observation of the noise peak at ∼−30 mT, which coincides with the center of the magnetic reversal region of the pinned layer. In this region, the noise level is enhanced significantly indicating magnetic fluctuations of the pinned layer are pronounced. Also, a much higher noise level was identified in the AP state compared to that in the RevP state [39], suggesting more remarkable magnetization fluctuation associated with the AP state. It is noted that the magnetic after effect may also contribute to the observed magnetic dependence of Hooge parameters in figure 3(b) [17]. However, the data presented in

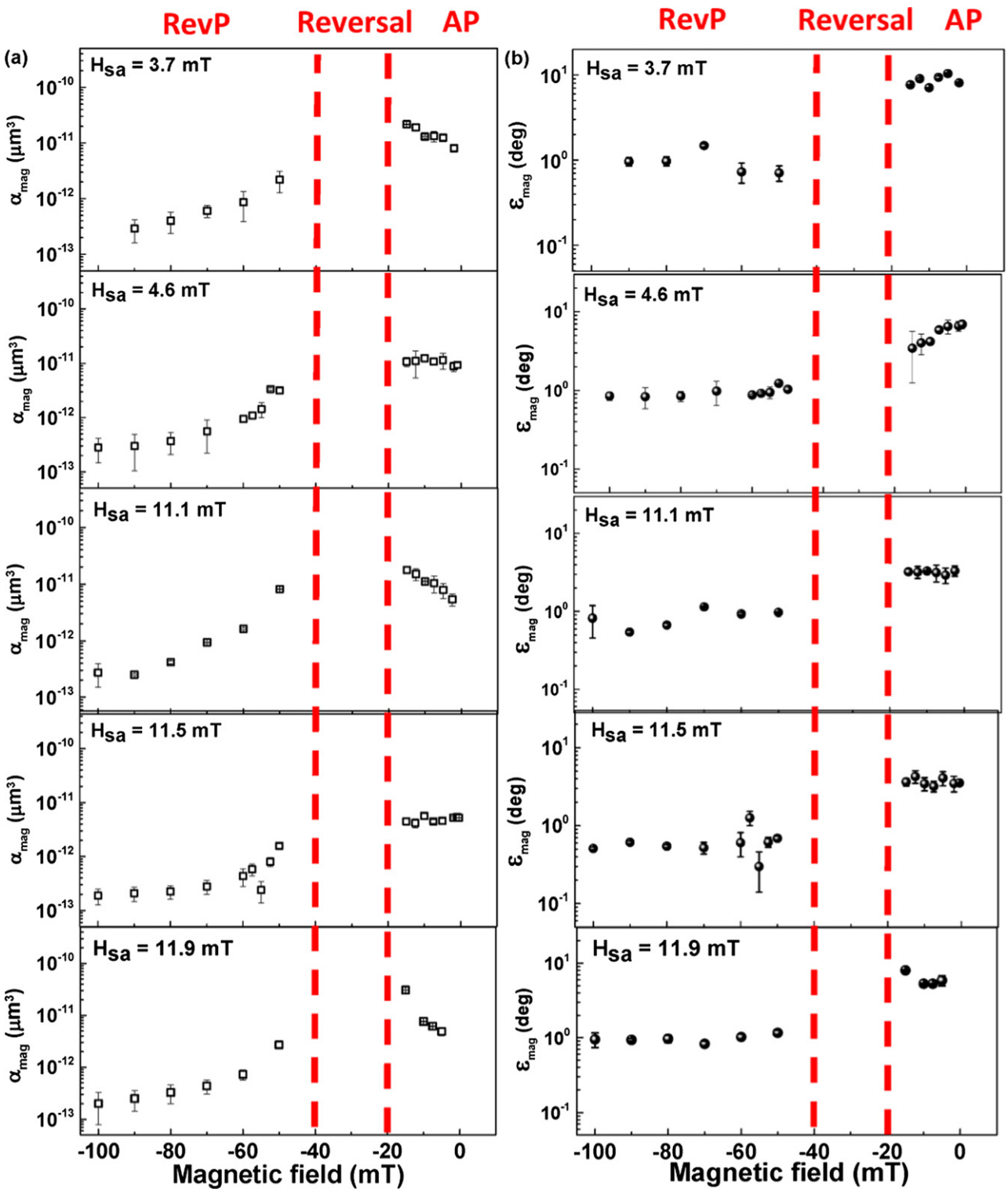

Figure 5. (a) Magnetic-field-dependence of the Hooge parameter (α_{mag}) of the MTJs with various shape anisotropies (H_{sa}) of the pinned layer, (b) magnetic field dependence of the magnetic phase loss ($\varepsilon_{\mathrm{mag}}$) of the MTJs with various shape anisotropies (H_{sa}) of the pinned layer.

this manuscript was believed to be the stationary noise instead of artifacts since the measurement in this manuscript was conducted after the magnetic aftereffect was well relaxed in 10 min (supplementary material).

To further investigate the magnetic noise of the MTJ, the values of α_{mag} were related to the MSP $= \frac{\Delta R}{R}(\frac{1}{R}\frac{\mathrm{d}R}{\mathrm{d}H})$ and the corresponding magnetic phase losses ($\varepsilon_{\mathrm{mag}}$). $\varepsilon_{\mathrm{mag}}$ was characterized by using the FDT [11, 18, 34], where R is the resistance of the MTJ, ΔR is the resistance difference between the P(RevP) and AP states, and $\frac{1}{R}\frac{\mathrm{d}R}{\mathrm{d}H}$ is the MTJ's homogeneous sensitivity [38]. In thermal equilibrium, the magnetic noise can be expressed by the following equation derived from the FDT

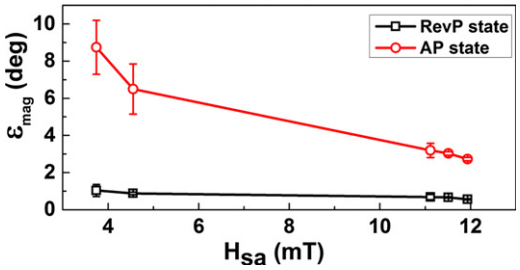

Figure 6. Magnetic phase loss (ε_{mag}) with respect to the shape anisotropy (H_{sa}) in the RevP and AP states.

[18, 40]:

$$\alpha_{mag} = \varepsilon_{mag}(H)\frac{k_B T}{\pi\mu_0 M_S}\frac{\Delta R}{R^2}\frac{dR}{dH}, \quad (2)$$

where k_B is the Boltzmann's constant, T is the temperature, μ_0 is the magnetic permeability of free space, and M_s is the saturation magnetization of the corresponding magnetic layer. In this MTJ, its pinned layer has a composite trilayer structure: CoFe thk_1/NiFeCuMo thk_2/CoFe thk_3, where thk_1, thk_2, and thk_3 are the thickness values of each layer. The saturation magnetization (M_s) of the pinned layer can be estimated by using the equation [36]:

$$M_S = \frac{\text{th}k_1 M_{sCoFe} + \text{th}k_2 M_{sNiFeCuMo} + \text{th}k_3 M_{sCoFe}}{\text{th}k_1 + \text{th}k_2 + \text{th}k_3}, \quad (3)$$

where M_{sCoFe} and $M_{sNiFeCuMo}$ denote the saturation magnetizations of CoFe and NiFeCuMo, respectively. The values of M_{sCoFe} and $M_{sNiFeCuMo}$ are 1592 emu/cm^3 and 616 emu/cm^3, respectively [41, 42]. The thickness values are thk_1 = 1.0 nm, thk_2 = 2.5 nm, and thk_3 = 0.5 nm for the experimental MTJ samples. Based on equation (3), the saturation magnetization of the pinned layer is therefore M_s = 982 emu/cm^3. As shown in figures 3(b) and (c), the MSP curve closely resembled the trend of α_{mag}. The ε_{mag} values with respect to the magnetic field were calculated using equation (2). As shown in figure 3(d), no noticeable field dependence of ε_{mag} was identified in the RevP and AP states, which was attributed to a nearly linear proportionality between α_{mag} and MSP. This observation indicated that the magnetization fluctuations were in thermal equilibrium regime in the RevP and AP magnetization alignments [11, 34]. Compared to the RevP state, the more remarkable magnetization fluctuation in the AP state also greatly enhanced the magnetic phase loss in the pinned layer and gave rise to relatively larger ε_{mag} values. When the magnetization configuration was switched from the RevP to AP state during the magnetic reversal process, a substantial change of ε_{mag} was identified, suggesting that the linear correlation between α_{mag} and MSP was no longer maintained.

To study the influencing factors of the magnetic noise, elliptical MTJs with different aspect ratios were fabricated, as illustrated in figure 1. Distinct demagnetizing factors arise from their different aspect ratios, which gives rise to a notable change in the effective shape anisotropy field of the pinned layer in these MTJs [43, 44]. Defining the length (l) and width (w) of the elliptical MTJ, one has its aspect ratio, $u = l/w$. The demagnetizing factors along the short axis (n_x) and long axis

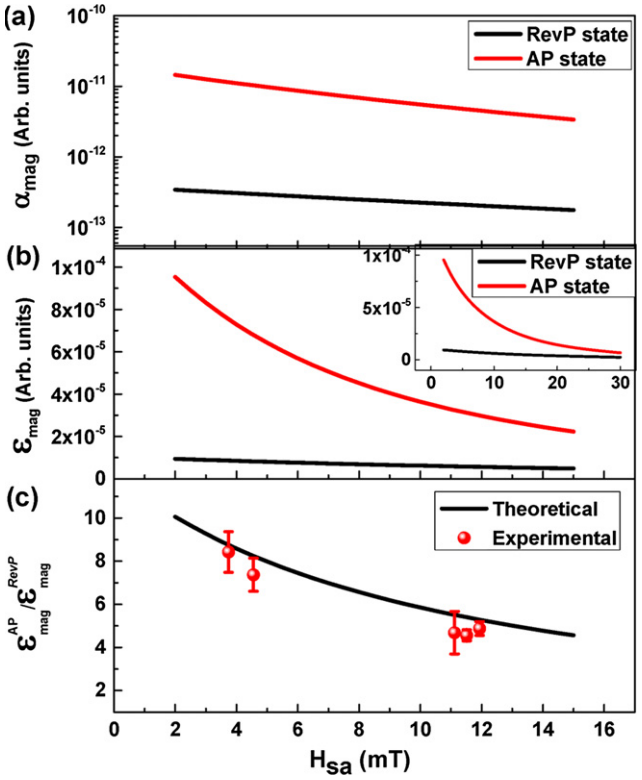

Figure 7. (a) Theoretically calculated noise power as a function of the shape anisotropy (H_{sa}) in the RevP ($H_{ext} \sim -100$ mT) and AP states ($H_{ext} \sim 0$ mT), (b) theoretically calculated magnetic phase loss (ε_{mag}) as a function of the shape anisotropy (H_{sa}) in the RevP ($H_{ext} \sim -100$ mT) and AP states ($H_{ext} \sim 0$ mT), inset is the calculated ε_{mag} with respect to a wider range of H_{sa}, (c) comparison of theoretical and experimental results on the ratio of magnetic phase losses ($\varepsilon_{mag}^{AP}/\varepsilon_{mag}^{RevP}$) in the AP and RevP states. The parameters used are $\alpha_1 = 0.01$, $T = 300$ K, $\gamma_0 = 1.76 \times 10^{11}$ Hz/T, $k_B = 1.38 \times 10^{-23}$ J/K, $M_{1s} = 982$ emu/cm^3.

(n_y) were calculated as

$$n_x = \frac{u}{2}\int_0^\infty \frac{1}{(u^2+s)\sqrt{(u^2+s)(1+s)s}}\,ds\cdot$$
$$n_y = \frac{u}{2}\int_0^\infty \frac{1}{(1+s)\sqrt{(u^2+s)(1+s)s}}\,ds \quad (4)$$

The effective shape anisotropy field (H_{sa}) was derived by inserting the equation (4) into the following expression

$$H_{sa} = 4\pi M_s \frac{thk}{w}(n_x - n_y), \quad (5)$$

where thk represents the thickness. The results are shown in figures 4(a) and (b), respectively. Upon increasing the aspect ratio, H_{sa} increased from ~4 mT to ~12 mT. A sharp enhancement of H_{sa} between the aspect ratio of 2.6 and 4.4 is due to the reduction of w from 10 μm to 5 μm.

The Hooge parameter (α_{mag}) and magnetic phase loss (ε_{mag}) of the fabricated MTJs with various shape anisotropy fields (H_{sa}) of the pinned layer were characterized, as shown in figures 5(a) and (b), respectively. Compared to the RevP state, the larger α_{mag} values in the AP state were attributed to the increase of the magnetic phase loss, which was confirmed

by the extraction of the ε_{mag} data for all MTJs (figure 5(b)). Upon increasing H_{sa}, a notable reduction of $\varepsilon_{mag}{}^{AP}$ in the AP state while a slight decrease of $\varepsilon_{mag}{}^{RevP}$ in the RevP state was observed (figure 6), revealing that the increase of the shape anisotropy caused a more pronounced suppression of the equilibrium magnetization fluctuations in the AP state. Furthermore, the increased H_{sa} also lessened the $\varepsilon_{mag}{}^{RV}$ in the magnetic reversal region of the pinned layer and diminished the substantial change of $\varepsilon_{mag}{}^{RV}$ when the magnetization configuration switched from the RevP to AP state in the magnetic reversal region (figure 5(b)). This phenomenon indicated that the magnetization fluctuations in the reversal region were also hindered due to the increase of the shape anisotropy.

4. Theoritical analysis

To unveil the underlying physical mechanism of the experimental observations, a macrospin model for describing the magnetization fluctuation in the pinned layer and free layer was constructed based on the FDT [15, 16]. The corresponding resistance noise power at P ($S_{R(RevP)}(\omega)$) and AP ($S_{R(AP)}(\omega)$) states were calculated as:

$$S_{R(RevP)}(\omega) = \frac{1}{\pi}\left[\frac{\partial R(\cos\ \theta_{RevP})}{\partial\ \cos\ \theta}\right]^2\left(\frac{\gamma_0 k_B T \alpha_1}{M_{1S}\Omega_1}\right)^2 \times \int_{-\infty}^{+\infty} \frac{(\gamma_0 {H_{xx}}^2 + v^2) \times [\gamma_0{}^2 {H_{xx}}^2 + (\omega - v)^2] + (\gamma_0{}^2 {H_{yy}}^2 + v^2) \times [\gamma_0{}^2 {H_{yy}}^2 + (\omega - v)^2] - 2\gamma_0{}^2 (H_{xx} + H_{yy})^2 v(\omega - v)}{\{(\gamma_0{}^2 H_{xx} H_{yy} - v^2)^2 + [\gamma_0 \alpha_1 (H_{xx} + H_{yy}) v]^2\} \times \{[\gamma_0{}^2 H_{xx} H_{yy} - (\omega - v)^2]^2 + [\gamma_0 \alpha_1 (H_{xx} + H_{yy})(\omega - v)]^2\}} \mathrm{d}v \tag{6}$$

$$S_{R(AP)}(\omega) = \frac{1}{\pi}\left[\frac{\partial R(\cos\ \theta_{AP})}{\partial\ \cos\ \theta}\right]^2\left(\frac{\gamma_0 k_B T \alpha_1}{M_{1S}\Omega_1}\right)^2 \times \int_{-\infty}^{+\infty} \frac{(\gamma_0 {H'_{xx}}^2 + v^2) \times [\gamma_0{}^2 {H'_{xx}}^2 + (\omega - v)^2] + (\gamma_0{}^2 {H'_{yy}}^2 + v^2) \times [\gamma_0{}^2 {H'_{yy}}^2 + (\omega - v)^2] - 2\gamma_0{}^2 (H'_{xx} + H'_{yy})^2 v(\omega - v)}{\{(\gamma_0{}^2 H'_{xx} H'_{yy} - v^2)^2 + [\gamma_0 \alpha_1 (H'_{xx} + H'_{yy}) v]^2\} \times \{[\gamma_0{}^2 H'_{xx} H'_{yy} - (\omega - v)^2]^2 + [\gamma_0 \alpha_1 (H'_{xx} + H'_{yy})(\omega - v)]^2\}} \mathrm{d}v \tag{7}$$

where $\frac{\partial R(\cos\ \theta_{RevP})}{\partial\ \cos\ \theta}$ and $\frac{\partial R(\cos\ \theta_{AP})}{\partial\ \cos\ \theta}$ represents the differential resistance at P and AP states, respectively. γ_0, k_B, α_1, M_{1s}, and Ω_1 are the gyrometric ratio of the electron, Boltzmann constant, damping parameter, saturation magnetization, and volume of the magnetization fluctuator, respectively. H_{xx} ($H_{xx}{}'$) and H_{yy} ($H_{yy}{}'$) stands for the effective field in the P and AP states:

$$\begin{aligned} H_{xx} &= H_{ext} + H_{sa} m_{1z} - H_{eb} + 4\pi m_{1z} M_{1s} \\ H_{yy} &= H_{ext} + H_{sa} m_{1z} - H_{eb} \\ H'_{xx} &= H_{ext} - H_{sa} m_{1z} - H_{eb} - 4\pi m_{1z} M_{1s} \\ H'_{yy} &= H_{ext} - H_{sa} m_{1z} - H_{eb} \end{aligned} \tag{8}$$

where H_{ext}, H_{sa}, H_{eb} are the external magnetic field, the shape anisotropy field and the exchange bias field. Details of the derivation procedures are presented in the supplementary material.

Based on the theoretical model, the effect of the shape anisotropy on the magnetic noise in both the RevP and AP magnetization states is demonstrated in figure 7(a). The resistance noise power was calculated by inserting all the related parameters into equations (6) and (7). Hooge parameter of the magnetic LFN was then estimated using equation (1). At low frequencies, higher noise level was identified in the AP state than that observed in the RevP state, which was coincident with the experimental observation (figure 5(a)). The increase of the shape anisotropy stabilized the magnetization fluctuation and led to a reduction in magnetic noise. Making use of the measured $\frac{\partial R(\cos\ \theta)}{\partial\ \cos\ \theta}$ data (the ratio of $\frac{\partial R(\cos\ \theta_{AP})}{\partial\ \cos\ \theta}/\frac{\partial R(\cos\ \theta_{RevP})}{\partial\ \cos\ \theta} \sim 2$) and inserting the calculated Hooge parameter into equation (2), the corresponding magnetic phase losses in the RevP and AP states were estimated (figure 7(b)). With the increase in the shape anisotropy field (H_{sa}), the calculated results confirmed that a more remarkable suppression of the magnetization fluctuation in the AP magnetization alignment was responsible for the steeper reduction of the magnetic phase loss in the AP state (ε_{mag}^{AP}). Upon further increasing the shape anisotropy field (H_{sa}) (inset of figure 7(b)), ε_{mag}^{AP} was further declined and its value tended to be comparable to that in the RevP state (ε_{mag}^{RevP}). For the MTJ with sufficiently large H_{sa}, the magnetic phase loss in the RevP and AP state could exhibit approximately equal values. In other words, the magnetic phase loss can be nearly constant over a wide magnetic field range from the RevP to AP state when H_{sa} of the MTJ is sufficiently large, indicating that the equilibrium magnetization fluctuation is maintained in all magnetization configurations. As illustrated in figure 7(c), the increased H_{sa} also significantly diminished the ratio of the magnetic phase losses ($\varepsilon_{mag}^{AP}/\varepsilon_{mag}^{RevP}$) in the AP and RevP states, which is in good agreement with the experimental observation.

5. Discussions

The macrospin model describes the effect of shape anisotropy on the MRTN due to fluctuation of pinned layer magnetization.

The theoretically calculated noise spectra from equations (6) and (7) exhibit a Lorentzian-like feature, having a frequency-independent plateau at low frequencies and a $1/f^2$ roll-off at high frequencies. The presence of the Lorentzian-like feature in the calculated spectra originates from modelling the pinned layer as a single macrospin. These Lorentzian-like MRTN noise spectra arising from a small number of large magnetic fluctuators have been demonstrated both in experiment and simulation [30, 45, 46]. In order to obtain the $1/f$ characteristic at low frequencies, a superposition of a large number of magnetic fluctuators with a certain energy distribution (e.g., lognormal distribution) are required to be considered in the model [45, 47]. The introduction of these individual magnetic fluctuators is physically reasonable because magnetic inhomogeneities existing in the magnetic layer can induce small magnetic domains whose magnetization directions are slightly misaligned with that of the total magnetization of the magnetic layer. Each misaligned magnetic domain can act as a magnetic fluctuator and produces a Lorentzian-like noise spectrum. The difference in the energy gap of magnetic fluctuators results in the varied probability of the two spin states in the measured time-domain RTN signals, and is thus responsible for the variations in roll-off frequencies in the frequency domain noise power spectra. The summation of noise spectra with different roll-off frequencies could result in a $1/f$ noise spectrum [30, 45].

6. Conclusion

In this work, the magnetic LFN of the MTJs with various shape anisotropies was investigated. The increase of the shape anisotropy stabilized the magnetization fluctuations of the pinned layer and led to a reduction in magnetic noise. Upon increasing the shape anisotropy, a notable suppression of the magnetic phase loss was identified in the AP state while it only exhibited a slight decrease in the RevP state. This suggested that the increase of the shape anisotropy caused a more pronounced reduction of the equilibrium magnetization fluctuations in the AP state, which was responsible for the steeper reduction of the magnetic phase loss in the AP state. The influence of the shape anisotropy on the magnetic noise was analytically described by constructing a macrospin model. This work has revealed the correlation between magnetic phase loss and magnetic LFN in the pinned layer. The comparison between experimental data and theoretical analysis gains insight in understanding the contribution of pinned layer fluctuation to the noise in AP and RevP states of MTJs.

Acknowledgments

This research is supported by the Seed Funding Program for Basic Research, Seed Funding Program for Applied Research and Small Project Funding Program from the University of Hong Kong, ITF Tier 3 funding (ITS-104/13, ITS-214/14), University Grants Committee of Hong Kong (AoE/P-04/08), RGC-GRF Grant of Hong Kong (HKU 17204617), National Natural Science Foundation of China (61804129, 61674124, 61774128, and 61874092), National Key Research and Development Program of China (2018YFB0406603), and Science and Technology Project of Fujian Province of China (2019H0002).

ORCID iDs

Xu Li https://orcid.org/0000-0002-0377-2925

References

[1] Parkin S S P, Kaiser C, Panchula A, Rice P M, Hughes B, Samant M and Yang S-H 2004 Giant tunnelling magnetoresistance at room temperature with MgO (100) tunnel barriers *Nat. Mater.* **3** 862

[2] Djayaprawira D D, Tsunekawa K, Nagai M, Maehara H, Yamagata S, Watanabe N, Yuasa S, Suzuki Y and Ando K 2005 230% room-temperature magnetoresistance in CoFeB /MgO/CoFeB magnetic tunnel junctions *Appl. Phys. Lett.* **86** 092502

[3] Yuasa S, Fukushima A, Kubota H, Suzuki Y and Ando K 2006 Giant tunneling magnetoresistance up to 410% at room temperature in fully epitaxial Co/MgO/Co magnetic tunnel junctions with bcc Co(001) electrodes *Appl. Phys. Lett.* **89** 042505

[4] Chaves R C, Freitas P P, Ocker B and Maass W 2008 MgO based picotesla field sensors *J. Appl. Phys.* **103** 07E931

[5] Fujiwara K, Oogane M, Yokota S, Nishikawa T, Naganuma H and Ando Y 2012 Fabrication of magnetic tunnel junctions with a bottom synthetic antiferro-coupled free layers for high sensitive magnetic field sensor devices *J. Appl. Phys.* **111** 07C710

[6] Cardoso S, Leitao D C, Gameiro L, Cardoso F, Ferreira R, Paz E and Freitas P P 2014 Magnetic tunnel junction sensors with pTesla sensitivity *Microsyst. Technol.* **20** 793

[7] Zheng C *et al* 2019 Magnetoresistive sensor development roadmap (non-recording applications) *IEEE Trans. Magn.* **55** 0800130

[8] Hu J-M, Li Z, Chen L-Q and Nan C-W 2011 High-density magnetoresistive random access memory operating at ultralow voltage at room temperature *Nat. Commun.* **2** 553

[9] Almeida J M, Ferreira R, Freitas P P, Langer J, Ocker B and Maass W 2006 1/f noise in linearized low resistance MgO magnetic tunnel junctions *J. Appl. Phys.* **99** 08B314

[10] Scola J, Polovy H, Fermon C, Pannetier-Lecœur M, Feng G, Fahy K and Coey J M D 2007 Noise in MgO barrier magnetic tunnel junctions with CoFeB electrodes: influence of annealing temperature *Appl. Phys. Lett.* **90** 252501

[11] Arakawa T *et al* 2012 Low-frequency and shot noises in CoFeB/MgO/CoFeB magnetic tunneling junctions *Phys. Rev.* B **86** 224423

[12] Nor A F M, Kato T, Ahn S J, Daibou T, Ono K, Oogane M, Ando Y and Miyazaki T 2006 Low-frequency noise in MgO magnetic tunnel junctions *J. Appl. Phys.* **99** 08T306

[13] Diao Z, Feng J F, Kurt H, Feng G and Coey J M D 2010 Reduced low frequency noise in electron beam evaporated MgO magnetic tunnel junctions *Appl. Phys. Lett.* **96** 202506

[14] Das B, Lee Y C, Li L C, Yi-Shiou L, Suen Y W, Horng L, Wu T, Chang C R and Wu J 2016 Low-frequency noise characterization of CoFeB/MgO/CoFeB MTJ-based perpendicular field sensor *IEEE Trans. Magn.* **52** 4001004

[15] Foros J, Brataas A, Bauer G E and Tserkovnyak Y 2007 Resistance noise in spin valves *Phys. Rev.* B **75** 092405

[16] Foros J, Brataas A, Bauer G E and Tserkovnyak Y 2009 Noise and dissipation in magnetoelectronic nanostructures *Phys. Rev.* B **79** 214407

[17] Guo F, McKusky G and Dahlberg E D 2013 Absence of magnetic state dependent low-frequency noise in spin-valve systems *Phys. Rev.* B **88** 014409

[18] Stearrett R, Wang W, Kou X, Feng J, Coey J, Xiao J and Nowak E 2012 Influence of exchange bias on magnetic losses in CoFeB/MgO/CoFeB tunnel junctions *Phys. Rev.* B **86** 014415

[19] Guo F, McKusky G and Dahlberg E D 2009 An investigation of the magnetic state dependent low frequency noise in magnetic tunnel junctions *Appl. Phys. Lett.* **95** 062512

[20] Huang L *et al* 2017 Noise suppression and sensitivity manipulation of magnetic tunnel junction sensors with soft magnetic $Co_{70.5}Fe_{4.5}Si_{15}B_{10}$ layer *J. Appl. Phys.* **122** 113903

[21] Dark J, Nunn G, Cressler J D, Davidović D and Davidović D 2019 Increasing the signal-to-noise ratio of magnetic tunnel junctions by cryogenic preamplification *J. Appl. Phys.* **125** 163902

[22] Hu J, Ji M, Qiu W, Pan L, Li P, Peng J, Hu Y, Liu H and Pan M 2019 Double-gap magnetic flux concentrator design for high-sensitivity magnetic tunnel junction sensors *Sensors* **19** 4475

[23] Wisniowski P, Dąbek M, Skowronski W, Stobiecki T, Cardoso S and Freitas P P 2014 Reduction of low frequency magnetic noise by voltage-induced magnetic anisotropy modulation in tunneling magnetoresistance sensors *Appl. Phys. Lett.* **105** 082404

[24] Luong V, Chang C, Jeng J, Lu C, Hsu J and Chang C 2014 Reduction of low-frequency noise in tunneling-magnetoresistance sensors with a modulated magnetic shielding *IEEE Trans. Magn.* **50** 4005904

[25] Okamoto K, Fuji Y, Higashi Y, Kaji S, Nagata T, Baba S, Yuzawa A and Hara M 2018 Enhanced annealing stability of exchange-biased pinned layer in magnetic tunnel junction using Ta/Ru/Ta/Ru underlayer *IEEE Trans. Magn.* **54** 4400404

[26] Chen J Y, Carroll N, Feng J F and Coey J M D 2012 Yoke-shaped MgO-barrier magnetic tunnel junction sensors *Appl. Phys. Lett.* **101** 262402

[27] Ozbay A, Gokce A, Flanagan T, Stearrett R A, Nowak E R and Nordman C 2009 Low frequency magnetoresistive noise in spin-valve structures *Appl. Phys. Lett.* **94** 202506

[28] Feng J, Diao Z, Kurt H, Stearrett R, Singh A, Nowak E R and Coey J M D 2012 Influence of growth and annealing conditions on low-frequency magnetic 1/*f* noise in MgO magnetic tunnel junctions *J. Appl. Phys.* **112** 093913

[29] Pipathanapoompron T, Stankiewicz A, Subramanian K, Grier A and Kaewrawang A 2020 Modeling of magnetic thermal noise in stable magnetic sensors *J. Appl. Phys.* **127** 073902

[30] Diao Z, Nowak E, Haughey K and Coey J 2011 Nanoscale dissipation and magnetoresistive 1/*f* noise in spin valves *Phys. Rev.* B **84** 094412

[31] Jiang L, Nowak E R, Scott P E, Johnson J, Slaughter J M, Sun J J and Dave R W 2004 Low-frequency magnetic and resistance noise in magnetic tunnel junctions *Phys. Rev.* B **69** 054407

[32] Herranz D, Gomez-Ibarlucea A, Schäfers M, Lara A, Reiss G and Aliev F G 2011 Low frequency noise due to magnetic inhomogeneities in submicron FeCoB/MgO/FeCoB magnetic tunnel junctions *Appl. Phys. Lett.* **99** 062511

[33] Heinonen O and Cho H S 2004 Thermal magnetic noise in tunneling readers *IEEE Trans. Magn.* **40** 2227

[34] Stearrett R, Wang W G, Shah L R, Xiao J Q and Nowak E R 2010 Magnetic noise evolution in CoFeB/MgO/CoFeB tunnel junctions during annealing *Appl. Phys. Lett.* **97** 243502

[35] Stearrett R, Wang W G, Kou X, Feng J F, Coey J M D, Xiao J Q and Nowak E R 2012 Influence of exchange bias on magnetic losses in CoFeB/MgO/CoFeB tunnel junctions *Phys. Rev.* B **86** 014415

[36] Yuan Z H *et al* 2016 Low frequency noise in magnetic tunneling junctions with $Co_{40}Fe_{40}B_{20}/Co_{70.5}Fe_{4.5}Si_{15}B_{10}$ composite free layer *J. Magn. Magn. Mater.* **398** 215

[37] Jiang L, Skovholt J F, Nowak E R and Slaughter J M 2004 Low-frequency magnetic and resistance noise in magnetoresistive tunnel junctions *Proc. SPIE* vol 13

[38] Wang X *et al* 2015 Ultrasensitive and broadband MoS2Photodetector driven by ferroelectrics *Adv. Mater.* **27** 6575

[39] Zhang Y and Xiao G 2019 Spin-dependent shot noise in MgO-based magnetic tunnel junctions under noncollinear magnetization alignment *Phys. Rev.* B **100** 224402

[40] Feng J F, Diao Z, Feng G, Nowak E R and Coey J M D 2010 Magnetic noise in MgO-based magnetic tunnel junction rings *Appl. Phys. Lett.* **96** 052504

[41] Egelhoff W F Jr, Pong P W T, Unguris J, McMichael R D, Nowak E R, Edelstein A S, Burnette J E and Fischer G A 2009 Critical challenges for picoTesla magnetic-tunnel-junction sensors *Sensors and Actuators* A **155** 217

[42] Qiu D Y, Ashraf K and Salahuddin S 2013 Nature of magnetic domains in an exchange coupled $BiFeO_3$/CoFe heterostructure *Appl. Phys. Lett.* **102** 112902

[43] Wiese N, Dimopoulos T, Rührig M, Wecker J and Reiss G 2005 Switching of submicron-sized, antiferromagnetically coupled CoFeB/Ru/CoFeB trilayers *J. Appl. Phys.* **98** 103904

[44] Sun J Z *et al* 2001 Thermal activation-induced sweep-rate dependence of magnetic switching astroid *Appl. Phys. Lett.* **78** 4004

[45] Wang L, Patwari M S and Stokes S W 2011 Modeling of 1/*f* noise due to thermally induced magnetic switches of antiferromagnetic grains in magnetic tunneling readers *J. Appl. Phys.* **109** 07B725

[46] Fischer M, Elm M T, Kato H, Sakita S, Hara S and Klar P J 2015 Analysis of magnetic random telegraph noise in individual arrangements of a small number of coupled MnAs nanoclusters *Phys. Rev.* B **92** 165306

[47] Leliaert J, Coene A, Liebl M, Eberbeck D, Steinhoff U, Wiekhorst F, Fischer B, Dupré L and Van Waeyenberge B 2015 Thermal magnetic noise spectra of nanoparticle ensembles *Appl. Phys. Lett.* **107** 222401